Zr-doping stabilizes spinel $LiMn_2O_4$ as a low cost long cycle life cathode for lithium ion batteries

Xiang-Gong Zhang(张祥功)[1], Wei Wu(吴伟)[2], Si-Si Zhou(周思思)[1,†], Fei Huang(黄飞)[2], Shi-Hao Xu(许诗浩)[2], Liang Yin(尹良)[2,3,‡], Wei Yang(杨伟)[2,§], and Hong Li(李泓)[2,3]

[1] *Wuhan Institute of Marine Electric Propulsion, Wuhan* 430064, *China*
[2] *Tianmu Lake Institute of Advanced Energy Storage Technologies Co., Ltd., Liyang* 213300, *China*
[3] *Institute of Physics, Chinese Academy of Sciences, Beijing* 100190, *China*

(Received 30 December 2022; revised manuscript received 30 January 2023; accepted manuscript online 6 February 2023)

The present commercial spinel $LiMn_2O_4$ delivers only 90 mAh/g–115 mAh/g, far lower than the theoretical specific capacity. It degrades fast caused by the Jahn–Teller effect, Mn dissolution and related side reactions that consume Li inventory. In this work, Zr doping is employed to improve the structural stability and electrochemical performance of spinel $LiMn_2O_4$. $Li_{1.06}Mn_{1.94-x}Zr_xO_4$ ($x = 0$, 0.01, 0.02, 0.04) have been successfully synthesized by a simple solid-state reaction method and evaluated as cathode for lithium ion batteries (LIB). $Li_{1.06}Mn_{1.92}Zr_{0.02}O_4$ is superior cathode material with a high capacity of 122 mAh/g at 1-C rate; long cycle stability, 98.39% retention after 100 cycles at 1-C rate, excellent high rate performance 107.1 mAh/g at 10-C rate, and high temperature performance 97.39% retention after 60 cycles. These are thought to be related to Zr doping effectively stabilizing the spinel $LiMn_2O_4$, by forming stronger Zr–O bonds in the octahedron, suppressing the Jahn–Teller effect, thus improving electrochemical performance.

Keywords: lithium battery, cathode, $LiMn_2O_4$, cycle life

PACS: 61.50.–f, 61.66.Fn, 82.47.Aa, 82.45.Fk **DOI:** 10.1088/1674-1056/acb919

1. Introduction

Energy storage technologies have to be much improved to meet the need of making full use of clean renewable energy in order to realize the goals of carbon neutral.[1,2] Lithium-ion batteries (LIB) is one of the best choices for energy storage considering energy density and technology readiness level so far.[3,4] The cathode material is the critical factor limiting the performance of LIB.[3,4] Spinel lithium manganese oxide ($LiMn_2O_4$) has the merits of high voltage, high rate, much safer, less toxic, and lower cost.[4–11] Thus it is advantageous over others in future large-scale energy storage applications, among the current dominant cathode materials used, especially considering resource availability and supply chain security. However, the present commercially available $LiMn_2O_4$ delivers only 110 mAh/g–120 mAh/g, far lower than its theoretical specific capacity of 148 mAh/g. Besides, the present LIB adopting $LiMn_2O_4$ faces the problem of fast decay mainly originating from itself such as the Jahn–Teller effect, Mn dissolution and related side reactions that consumes electrolyte.[12] High-temperature application environment will aggravate the situation. Advanced characterization techniques and mechanism investigation are of significance.[13–16] Electrolyte improvement with new solvents and additives are promising strategies.[17] For $LiMn_2O_4$ improvement, doping and coating are common strategies suggested to stable its structure and elongate cycle performance. Doping with foreign ions, including cations such as Li^+, Na^+, Mg^{2+}, Zn^{2+}, Cu^{2+}, Ni^{2+}, Al^{3+}, Fe^{3+}, Co^{3+}, Cr^{3+}, Ga^{3+}, La^{3+}, Ce^{3+}, Nd^{3+}, and also anions F^-, S^{2-}, B^{3-} have been reported to effectively improving cycle life.[7–11,14,18–31] Most of those ions (*e.g.*, Cu^{2+}, Ni^{2+}, Co^{3+}, Cr^{3+}) preferred to occupy 16*d* sites, substituting Mn^{3+}, increasing the average valence of Mn to over 3.5, while some (*e.g.*, Zn^{2+} and Ga^{3+}) preferred to 8*a* sites.[11] So the occupying of the dopant determines the structural stability and electrochemical performance such as discharge specific capacity and cycle performance at room temperature and high temperature. High valence ions such as Ti^{4+}, Si^{4+}, Zr^{4+}, Nb^{5+} were also reported to be reasonable dopant for modifying $LiMn_2O_4$.[19,21,22,27,28,30] But the doping mechanism, crystalline structure evolution and electrochemical performance of some systems were still not clear. As it is a consensus that the Li/Mn ratio in $LiMn_2O_4$ is critical in industry applications, as a partial substitute of Mn^{3+} at 16*d* site using Li in $LiMn_2O_4$ favors cycle performance with a certain degree of capacity loses.[11]

In the present study, we chose to further substitute part of manganese in $LiMn_2O_4$ with zirconium (ZrO_2), $Li_{1.06}Mn_{1.94-x}Zr_xO_4$ ($x = 0$, 0.01, 0.02, 0.04) to examine the effects of tetravalent cation, both crystal structure and electrochemical performance. Results demonstrate that Zr doping can improve specific capacity to 132.1 mAh/g at a very low

†Corresponding author. E-mail: zhousisi18@126.com
‡Corresponding author. E-mail: lyin@iphy.ac.cn
§Corresponding author. E-mail: billwyang@163.com

© 2023 Chinese Physical Society and IOP Publishing Ltd

dose. While, increasing dopant dose can enhance rate performance (107.1 mAh/g at 10-C rate), capacity retention remarkably both at room temperature (98.39% retention after 100 cycles at 1-C rate) and high temperature (97.39% retention after 60 cycles 1-C rate at 45 °C), without significant scarifying specific capacity. Analysis results suggest that Zr-doping stabilizes the MnO_6 octahedron by forming a stronger Zr–O bond over the Mn–O bond, which helps alleviate the adverse impact of the Jahn–Teller effect.

2. Experiment details

2.1. Materials

Zirconium-doped $LiMn_2O_4$ cathode materials,

$$Li_{1.06}Mn_{1.94}O_4 \text{ (LMO-Zr-0.00)},$$
$$Li_{1.06}Mn_{1.93}Zr_{0.01}O_4 \text{ (LMO-Zr-0.01)},$$
$$Li_{1.06}Mn_{1.92}Zr_{0.02}O_4 \text{ (LMO-Zr-0.02)},$$
$$Li_{1.06}Mn_{1.90}Zr_{0.04}O_4 \text{ (LMO-Zr-0.04)}$$

were synthesized by solid-state reaction method. Commercial spherical Mn_3O_4 (98.5%, SINOSTEEL, Maanshan, Anhui), battery grade Li_2CO_3 (99.5%, Nanshi, Jiangxi) and nano ZrO_2 (99%, Xuancheng Jingrui New Materials Co., Ltd., Anhui) were used as starting materials and used as received without further treatment.

Materials were weighted according to the designed stoichiometry and then thoroughly mixed by dry ball milling for 60 min at a rotate speed of 250 rpm using polyurethane balls. The resulting mixtures were heated to 770 °C with a heat-up speed of 5 °C/min, and calcined for 20 hours before naturally cooling to room temperature. Compressed air flow was provided at a speed of 1.5 L/min for the sintering process. The obtained materials were sieved using a 200-mesh sieve before the test.

2.2. Cell assembling

To prepare the $LiMn_2O_4$ cathode electrode, $LiMn_2O_4$, super P (Timcal) and PVDF (5230, Solvay) were first dispersed by a weight ratio of 90:5:5 using N-methyl pyrrolidone (NMP, 99%, Aladdin) solvent. The obtained slurry was then coated evenly on aluminum foil to produce the green cathode film. The cathode films were then dried at 110 °C for 12 hours in a vacuum oven before use. The diameter of the electrode was 12 mm with active material loading of about 5 mg/cm^{-2}. The CR2032 coin cells were assembled in an argon-filled glove box ($H_2O < 0.1$ ppm and $O_2 < 0.5$ ppm) using lithium foil as an anode, $LiMn_2O_4$ cathode electrode and PP separator (25 μm). The electrolyte 1-M LiPF6 in EC/DEC/EMC (1:1:1 in volume) was purchased from Dongguan Shanshan, and 70 μl of electrolyte was injected in each cell. All the cells were settled for 6 hours before the test to ensure adequate infiltration.

2.3. Electrochemical test

Cyclic voltammetry was conducted from 3 V to 4.5 V with different scan rates of 0.1 mV/s, 0.2 mV/s, 0.4 mV/s, 0.5 mV/s, 0.8 mV/s, and 1 mV/s on an Arbin LBT20084 cell tester. The galvanostatic charge/discharge cycling between 3 V–4.3 V was performed on the LAND BT2000 battery tester. For cycle and rate performance investigation. The cells were activated at 0.1 C for one cycle before subsequent cycles (1 C and 5 C) and rates (0.1 C, 0.2 C, 0.5 C, 1 C, 2 C, 5 C, 10 C, 0.1 C) evaluations. Electrochemical impedance spectrums (EIS) were conducted on Zahner Ennium pro electrochemical work station in the frequency range of 0.01 Hz to 10^6 Hz, with a 5-mV AC voltage perturbation.

2.4. Characterization

The $LiMn_2O_4$ cathode materials were measured by powder x-ray diffraction (XRD, Bruker D8 Advanced) to identify phase and analysis crystal structure evolution. Morphology and microstructure were studied on scanning electron microscopy (SEM, Hitachi Regulus8100) and transmission electron microscopy (TEM, JEM-F200). Energy dispersive spectroscopy (EDS) amounted on SEM was employed to inquire about the element mapping over the cathode samples. Raman spectrums were investigated on a Renishaw Invia reflex Raman microscope.

3. Results and discussion

3.1. Crystal structure analysis

The phase purity of nominal zirconium-doped $Li_{1.06}Mn_{1.94-x}Zr_xO_4$ ($x = 0$, 0.01, 0.02, 0.04) cathode materials as synthesized are investigated using powder x-ray diffraction (XRD) technique. As shown in Fig. 1(a), the main diffraction peaks are identified to cubic spinel phase ($Fd\bar{3}m$) $LiMn_2O_4$ (match well with JCPDS No. 035-0782). The diffraction peaks corresponding to (111), (311), (222), (400), (331), (333), (440), and (531) crystal planes are clearly observed for all the obtained samples. The cubic structural lattice constants are further analyzed by Rietveld analysis. The simulated patterns and parameters are presented in Fig. 1 and Table 1. The patterns are well-refined considering Zr taking the 16*d* site, see Figs. 1(c)–1(f) and Table 1. The lattice constants are 8.23775 Å, 8.23314 Å, 8.23202 Å, and 8.22986 Å for LMO-Zr-0.00, LMO-Zr-0.01, LMO-Zr-0.02, and LMO-Zr-0.04 respectively, decreased from 8.23314 Å to 8.22986 Å along with the increasing of Zr doping concentration. And so are the Mn/Zr–O bonds, for LMO-Zr-0.00, LMO-Zr-0.01, and LMO-Zr-0.02, except for nominal LMO-Zr-0.04, see Table 1. Theoretically, Li, Mn, and O atoms are situated at 8*a*, 16*d*, and 32*e* sites respectively in spinel $LiMn_2O_4$.[4,5,11] However, Li and Mn atoms are usually forming anti-site to a certain extent, *i.e.*, part of Li occupies 16*d* site and otherwise some Mn locate

at 8*a* sites, due to the imperfect of precursor and synthesis conditions, which may block the movement of conduction Li ions thus cause capacity lose and other electrochemical degradation. In this work, Zr atoms are thought to partially substitute Mn at the 16*d* site. The well-refined results confirm this configuration. The refined occupying values of the 8*a* site suggest that zirconium doping reduces the relative occupying degree of Mn at the Li_8*a* site. This configuration may favor the diffusion of Li ions. These facts suggest that zirconium doping strengthens MO_6 octahedral through stronger Zr–O bond, considering the high Zr–O bonding energy than that of Mn–O, which may help maintain the structural integrity and improve cycle performance of $LiMn_2O_4$ cathode. The ratio of peak intensity $I(311)/I(400)$ was calculated and listed in Table 1. Results show that zirconium doping may be beneficial to the cycle stability improvement of $LiMn_2O_4$ cathode, according to previous reports.[32] Very weak peaks at $2\theta = 28.22°$ and 31.84° are detected in LMO-Zr-0.02, and become stronger in LMO-Zr-0.04, see Fig. 1(a), which are attributed to ZrO_2. The ZrO_2 is originated from the un-reacted dopant. The results indicate that a small part of the ZrO_2 dopant was not diffused into the parent $LiMn_2O_4$ under these calcination conditions. This fact is also confirmed by SEM and TEM characterizations in the next section. As a result, the actual Li/Mn ratio in nominal LMO-Zr-0.04 is higher than the designed 1.06, which means more Li atoms occupy the Mn_16*d* site thus leading to longer Mn–O length. This explains the anomaly in the refined results including Mn–O bond length, occupying degree of Mn at Li_8*a* site, and R_{Bragg} for nominal LMO-Zr-0.04 compared to that of LMO-Zr-0.00, LMO-Zr-0.01, and LMO-Zr-0.02.

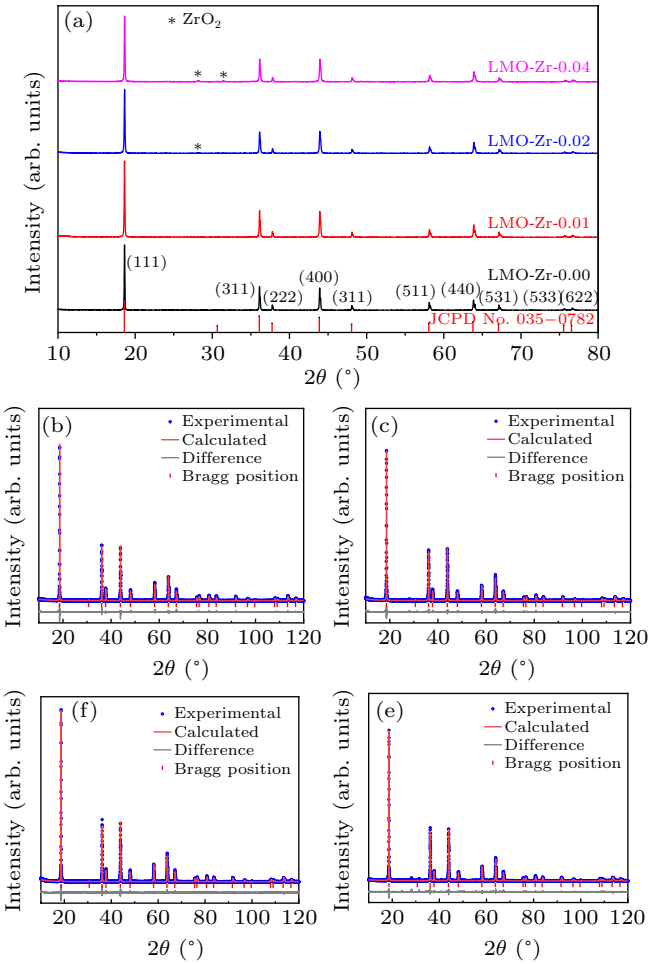


Fig. 1. XRD patterns (a), and [(b)–(e)] refined XRD data of nominal Zr-doped $Li_{1.06}Mn_{1.94-x}Zr_xO_4$ ($x = 0$, 0.01, 0.02, 0.04) cathodes calcined at 770 °C for 20 h in air, (b) LMO-Zr-0.00, (c) LMO-Zr-0.01, (d) LMO-Zr-0.02, (e) LMO-Zr-0.04.

Table 1. Crystal structural parameters of $Li_{1.06}Mn_{1.94-x}Zr_xO_4$ cathode ($x = 0$, 0.01, 0.02, 0.04).

Sample	Lattice constant *a* (Å)	Unit cell volume (Å^3)	R_{Bragg}	O*x*	Occ_Li_8*a*	Occ_Mn_16*d*	Mn–O length (Å)	$I(311)/I(400)$
LMO-Zr-0.00	8.23775	559.018	3.30	0.23797	1.27152	0.99824	1.9653(12)	1.078
LMO-Zr-0.01	8.23314	558.080	2.34	.23702	1.06745	0.94050	1.9572(11)	0.996
LMO-Zr-0.02	8.23202	557.852	2.08	0.23705	1.08051	0.93742	1.9572(11)	0.968
LMO-Zr-0.04	8.22986	557.413	2.67	.23797	1.11646	0.93402	1.9635(12)	0.993

3.2. Morphologies analysis

Morphologies of the as-synthesized cathode materials are studied using field emission scanning electron microscopy (SEM) and transmission electron microscopy (TEM). As shown in Figs. 2(a)–2(d), the cathode materials are all secondary spherical particles, made of primary nano-crystals, with a diameter of about 6 μm–12 μm. The spherical structure here born from the spherical Mn_3O_4 precursor used, will reduce the effective contact area with liquid electrolyte. Therefore, alleviates Mn dissolution and related side reactions, which is critical for $LiMn_2O_4$ when we are aiming at elongating the electrochemical cycle capability. Zr was evenly diffused into the parent materials as confirmed by both SEM/EDS Figs. 2(e) and 2(f) and TEM/EDS Figs. 2(i)–2(l). It is notable that there were nano particles attached on the surface when comparing the doped cathodes, Fig. 2(h), and the undoped cathode, Fig. 2(g). And the amount of nano particles increase upon the increasing of zirconium doping concentration Figs. 2(b)–2(d), which are identified to be the unreacted dopant ZrO_2, as presented in Figs. 2(i)–2(l). This observation is consistent with the XRD analysis mentioned above. So, the calcination condition we employed lead to composite cathodes, *i.e.*, the obtained cathode is actually zirconium-doped and unintended partial isolated coated, and doping domains. Doping stabilizes crystal structure and coating reduces surficial reactions, both of which are beneficial to improve the cycle performance of the cathode.

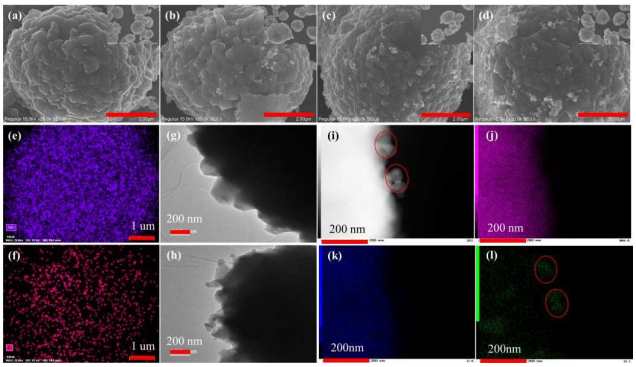


Fig. 2. The SEM and TEM images of as-synthesized nominal Zr-doped $Li_{1.06}Mn_{1.94-x}Zr_xO_4$ ($x = 0$, 0.01, 0.02, 0.04) cathodes. (a) and (e) LMO-Zr-0.00; (b) and (f) LMO-Zr-0.01; (c) and (g) LMO-Zr-0.02; (d) and (h) LMO-Zr-0.04; SEM/EDS mapping of (e) Mn and (f) Zr element; TEM/EDS mapping of (j) Mn, (k) O, and (l) Zr element corresponding to the selected area in panel (i); (a)–(d) and the insertions in panels (a)–(d) are SEM images in the larger area taken at lower magnification rate for the corresponding cathode materials; And panels (g)–(h) are TEM images. The red cycles in panels (i) and (l) are marked to illustrate the nano ZrO_2 particle.

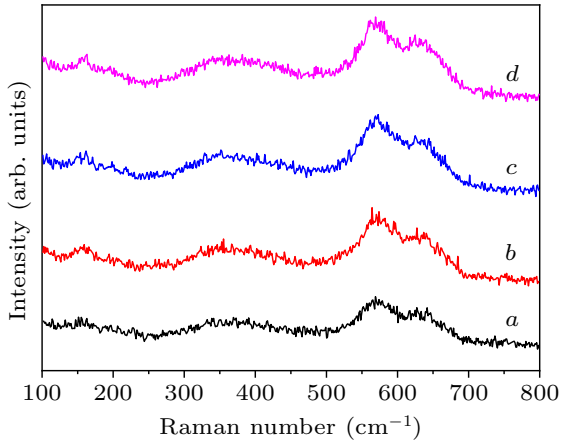


Fig. 3. The Raman spectrums of Zr-doped cathodes: curve *a* LMO-Zr-0.00, curve *b* LMO-Zr-0.01, curve *c* LMO-Zr-0.02, and curve *d* LMO-Zr-0.04.

Raman spectrum is often used to characterize the vibration mode of chemical bonded atoms in the crystal. The curves *a*–*d* in Fig. 3 are the Raman spectrums recorded from 100 cm^{-1} and 800 cm^{-1}. The spectrums showed high-frequency vibrational bands around 620 cm^{-1}–660 cm^{-1} and 560 cm^{-1}–590 cm^{-1}, and medium frequency vibrational band around 300 cm^{-1}–400 cm^{-1} and low-frequency bands at about 160 cm^{-1}. The vibration mode of spinel $LiMn_2O_4$ in the Raman spectrum was reported previously.[16,33–36] The low wavenumber at around 160 cm^{-1} is unexpected and not experimentally reported as far as we know, which might be originated from the Li deficient $Li_{0.5}Mn_2O_4$ phase.[33–35] The medium frequency peak located between 300 cm^{-1}–400 cm^{-1} is related to Li–O vibration. The strong band at 627 cm^{-1}–640 cm^{-1} is assigned to Mn–O symmetric stretching mode in MnO_6 octahedron. The band peaks shift to higher wave number upon zirconium doping, which may be attributed to the shortness of the bond and stronger Zr–O bond compared to Mn–O in the octahedron. And a maximum of 6 cm^{-1} shift was observed for LMO-Zr-0.02. This result suggests that LMO-Zr-0.02 is potentially stable for the electrochemical cycle, and is consistent with the results derived from XRD data refinement.

3.3. Electrochemical charge–discharge assessment

Cyclic voltammetry (CV) analyses in a range of 3.0 V–4.5 V were conducted to study the oxidation and reduction potentials for the $Li_{1.06}Mn_{1.94}O_4$ and Zr-doped $LiMn_2O_4$ cathode materials, displayed in Fig. 4(a). Two oxidative peaks and two reductive peaks are observed, corresponding to Li-ion extraction and intercalation process. The oxidative and reductive potentials for LMO-Zr-0.00 are 4.13 V, 4.25 V, and 3.88 V, 4.03 V respectively. Whereas, Zr-doped $LiMn_2O_4$ cathodes LMO-Zr-0.01, LMO-Zr-0.02, and LMO-Zr-0.04 have higher oxidative potentials. Meanwhile, larger oxidative currents are observed for LMO-Zr-0.01 and LMO-Zr-0.02 compared to LMO-Zr-0.00, and LMO-Zr-0.04 delivers the lowest oxidation current. Moreover, LMO-Zr-0.01 and LMO-Zr-0.02 cathodes display a large capacity than the other two cathodes. These results indicate that LMO-Zr-0.01 and LMO-Zr-0.02 cathodes have superior lithium-ion extraction and intercalation dynamics than LMO-Zr-0.00 and LMO-Zr-0.04.

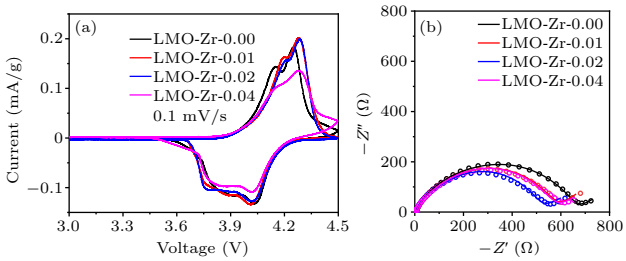


Fig. 4. (a) The *C*–*V* profiles at scan 0.1-mV/s rate and (b) Nyquist plots of coin cells based on LMO-Zr-0.00, LMO-Zr-0.01, LMO-Zr-0.02, and LMO-Zr-0.04 cathode materials.

The galvanostatic charge/discharge performance of the calcined cathode materials was conducted using different C-rates at room temperature and high temperature (45 °C). Constant current and constant voltage (CCCV) charging mode for the charging process (charging ended at 0.05 C) and constant current (CC) for discharging process were used. The initial charge/discharge profiles, initial columbic efficiency, discharge capacity retention, and rate performance are demonstrated in Fig. 5. There are two discharge plateaus located around 3.95 V and 4.09 V, two charge plateaus around 4.04 V and 4.17 V respectively for LMO-Zr-0.00 material. LMO-Zr-0.01 and LMO-Zr-0.02 materials have larger discharge voltage and lower charge voltage, *i.e.*, smaller over-potential, indicating faster Li ion extraction/intercalation performance. This is consistent with oxidation/reduction profiles displayed in the CV analysis.

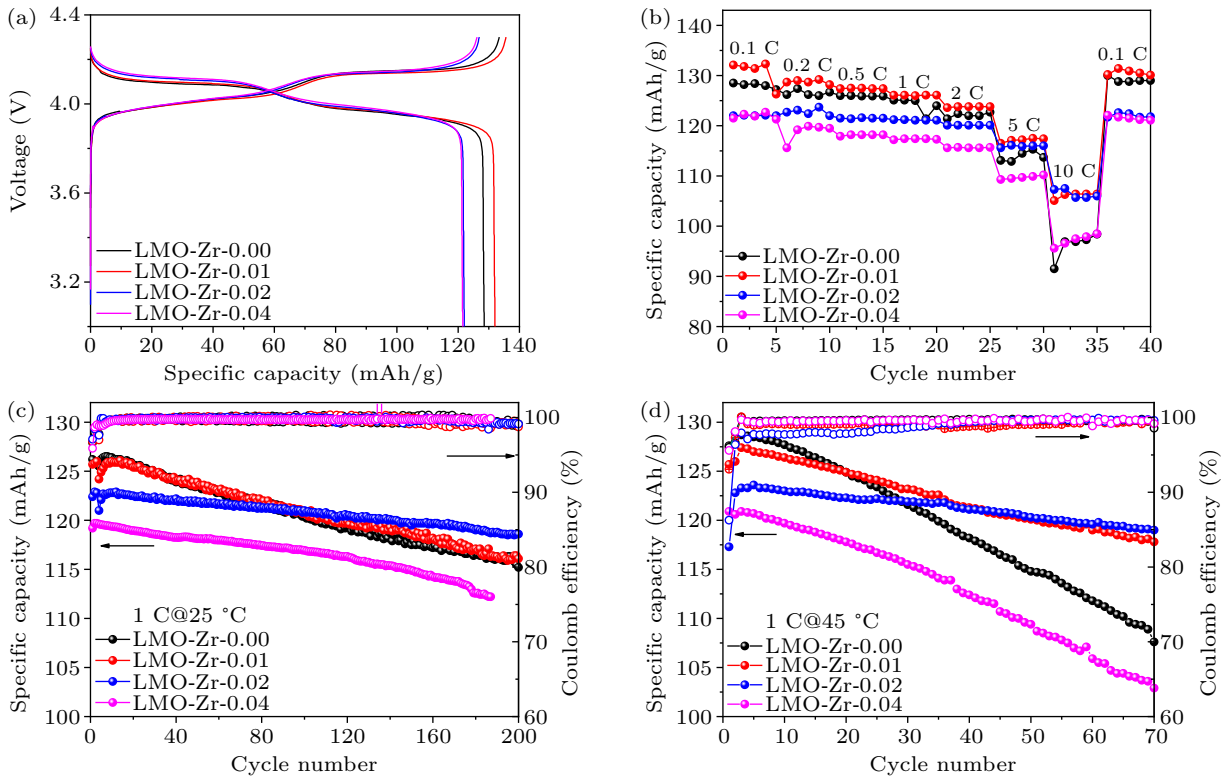


Fig. 5. Galvanostatic charge–discharge of Zr-doped cathodes (a) the first charge–discharge curves at 0.1 C at room temperature, (b) rate performance at room temperature, (c) 1-C cycle at room temperature, the cell for LMO-Zr-0.00 was intentionally stopped as it dived at about 180 cycles, (d) 1-C cycle at 45-°C high temperature.

The specific discharge capacity of LMO-Zr-0.01 is 132.1 mAh/g, surpassing that of LMO-Zr-0.00 at 128.5 mAh/g at 0.1 C, while that are 122.0 mAh/g and 121.5 mAh/g for LMO-Zr-0.02 and LMO-Zr-0.04. The initial columbic efficiencies are 96.32%, 97.41%, 96.13%, and 96.35% respectively. The EIS measured after the first two cycles displayed in Fig. 4(b) demonstrates that LMO-Zr-0.01 and LMO-Zr-0.02 cathodes are favorable from the aspect of impedance, and LMO-Zr-0.02 cathode has the smallest impedance. The specific capacities are 125.1 mAh/g, 126.1 mAh/g, 121.2 mAh/g, and 117.4 mAh/g at a 1-C rate, much higher than the most of the available commercial $LiMn_2O_4$ cathode materials. LMO-Zr-0.01 and LMO-Zr-0.02 materials show excellent rate performance and obvious advantage over LMO-Zr-0.00 and LMO-Zr-0.04, when the rate increased to 10 C, they still deliver 105.1 mAh/g and 107.3 mAh/g respectively. The capacity retentions are 95.80%, 95.80%, 98.39%, and 97.72% for 100 cycles at 1 C at room temperature. And capacity retention is still 97.31% for LMO-Zr-0.02 after 200 cycles, which is the highest for all the four cathodes. When subjected to an environmental case of 45 °C, all the four cathode materials demonstrate high specific discharge capacities, 128.7 mAh/g, 127.4 mAh/g, 123.3 mAh/g, 120.9 mAh/g respectively for LMO-Zr-0.00, LMO-Zr-0.01, LMO-Zr-0.02, LMO-Zr-0.04, comparable to that at room temperature. Moreover, LMO-Zr-0.02 shows better capacity retention over the others, 97.39% after 60 cycles. These results together confirm that LMO-Zr-0.02 is a cathode material with high specific and long life, which originates from the simple zirconium doping, and is related to its stabilized structure.

4. Conclusion

In summary, Zr-doped spinel $Li_{1.06}Mn_{1.94-x}Zr_xO_4$ (x = 0, 0.01, 0.02, 0.04) have been successfully synthesized by a simple solid-state reaction method. Zr doping stabilizes the $LiMn_2O_4$ by stronger Zr–O bonds in the octahedron, thus improving electrochemical performance. Zr doping at a lower level improves the specific capacity (132.1 mAh/g for $Li_{1.06}Mn_{1.93}Zr_{0.01}O_4$, surpassing that of $Li_{1.06}Mn_{1.94}O_4$, 128.5 mAh/g at 0.1 C), increasing the doping level will reduce the capacity (122.0 mAh/g and 121.5 mAh/g for $Li_{1.06}Mn_{1.92}Zr_{0.02}O_4$ and $Li_{1.06}Mn_{1.90}Zr_{0.04}O_4$), but will further promote the stability of $LiMn_2O_4$. $Li_{1.06}Mn_{1.92}Zr_{0.02}O_4$ is a superior cathode material candidate with high capacity, long stability, excellent high rate performances, and high-temperature performance. It is thought to be the balance point of high specific capacity and cycle stability. To verify on large scale quantity synthesis and assessment in commercial-level cells is being promoted for practical applications.

Acknowledgments

Project supported by research on high power flexible battery in all sea depth (Grant No. 2020-XXXX-XX-246-00).

References

[1] Wang F, Harindintwali J D and Yuan Z, *et al.* 2021 *Innovation* **2** 100180
[2] Lin R and Ren J 2020 *Renewable Energy and Sustainable Development* **6** 3
[3] Tarascon J M and Armand M 2001 *Nature* **414** 359
[4] Thackeray M M and Amine K 2021 *Nature Energy* **6** 566
[5] Eriksson T 2001 *LiMn2O4 as a Li-Ion Battery Cathode: From Bulk to Electrolyte Interface* (Uppsala Universitet)
[6] Thackeray M M 1997 *Manganese oxides for lithium batteries*, Vol. 25 pp. 1–71
[7] Yoshio M, Noguchi H, Xia Y and Ikeda K 1996 *Denki Kagaku* **64** 123
[8] Xia Y and Yoshio M 1995 *Journal of Power Sources* **57** 125
[9] Xia Y and Yoshio M 1997 *Journal of Power Sources* **66** 129
[10] Xia Y, Hideshima Y, Kumada N, Nagano M and Yoshio M 1998 *Journal of Power Sources* **74** 24
[11] Xia Y and Yoshio M 2003 *Lithium Batteries: Science and Technology*, eds. Nazri G A and Pistoia G (Boston, MA: Springer US) pp. 361–380
[12] Tang D, Sun Y, Yang Z, Ben L, Gu L and Huang X 2014 *Chemistry of Materials* **26** 3535
[13] Sun Z, Li M, Xiao B, Liu X, Lin H, Jiang B, Liu H, Li M, Peng D L and Zhang Q 2022 *eTransportation* **14** 100203
[14] Wang R, Chen X, Huang Z, Yang J, Liu F, Chu M, Liu T, Wang C, Zhu W, Li S, Li S, Zheng J, Chen J, He L, Jin L, Pan F and Xiao Y 2021 *Nat. Commun.* **12** 3085
[15] Chudzik K, Świętosławski M, Bakierska M, Kubicka M, Natkański P, Kawałko J and Molenda M 2021 *Electrochimica Acta* **373** 137901
[16] Ramana C V, Massot M and Julien C M 2005 *Surf. Interface Anal.* **37** 412
[17] Jiang B, Li J, Luo B, Yan Q, Li H, Liu L, Chu L, Li Y, Zhang Q and Li M 2021 *Journal of Energy Chemistry* **60** 564
[18] Wen W, Ju B, Wang X, Wu C, Shu H and Yang X 2014 *Electrochimica Acta* **147** 271
[19] Ji H, Ben L, Wang S, Liu Z, Monteiro R, Ribas R, Yu H, Gao P, Zhu Y and Huang X 2021 *ACS Appl. Energy Mater.* **4** 8350
[20] Yu Y, Xiang M, Guo J, Su C, Liu X, Bai H, Bai W and Duan K 2019 *Journal of Colloid and Interface Science* **555** 64
[21] Liu X, Wang J, Zhang J and Yang S 2006 *Journal of Materials Science: Materials in Electronics* **17** 865
[22] Ramogayana B, Maenetja K P and Ngoepe P E 2022 *Suid-Afrikaanse Tydskrif vir Natuurwetenskap en Tegnologie* **40** 22
[23] Ram P, Singhal R, Choudhary G and Sharma R K 2017 *Journal of Electroanalytical Chemistry* **802** 94
[24] Guohua L, Ikuta H, Uchida T and Wakihara M 1996 *Journal of The Electrochemical Society* **143** 178
[25] Fu Y, Jiang H, Hu Y, Dai Y, Zhang L and Li C 2015 *Industrial and Engineering Chemistry Research* **54** 3800
[26] Hou Y, Chang K, Tang H, Li B, Hou Y and Chang Z 2019 *Electrochimica Acta* **319** 587
[27] Li Y, Zhu G, Ran Q, Liu J, Zhou Y, Zhao M, Cao P and Zhao H 2021 *International Journal of Electrochemical Science* **16** 1
[28] Zhao H, Li F, Bai X, Wu T, Wang Z, Li Y and Su J 2018 *Materials* **11** 1302
[29] Zhao H, Bai X, Wang J, Li D, Li B, Wang Y, Dong L, Liu B and Komarneni S 2018 *Materials* **11** 1558
[30] Zhao H, Liu S, Wang Z, Cai Y, Tan M and Liu X 2016 *Electrochimica Acta* **199** 18
[31] Li L, Fu L, Li M, Wang C, Zhao Z, Xie S, Lin H, Wu X, Liu H, Zhang L, Zhang Q and Tan L 2022 *Journal of Energy Chemistry* **71** 588
[32] Todorov Y M, Hideshima Y, Noguchi H and Yoshio M 1999 *Journal of Power Sources* **77** 198
[33] Julien C 2003 *Solid State Ionics* **159** 345
[34] Murali N, Margarette S J and Veeraiah V 2016 *IOP Conference Series: Materials Science and Engineering* **149** 012193
[35] Ammundsen B, Burns G R, Islam M S, Kanoh H and Rozière J 1999 *J. Phys. Chem. B* **103** 5175
[36] Baddour-Hadjean R and Pereira-Ramos J P 2010 *Chem. Rev.* **110** 1278